Coating Graphene Paper with 2D-Assembly of Electrocatalytic Nanoparticles: A Modular Approach toward High-Performance Flexible Electrodes

Fei Xiao, Jibin Song, Hongcai Gao, Xiaoli Zan, Rong Xu, and Hongwei Duan*

School of Chemical and Biomedical Engineering, Nanyang Technological University, 70 Nanyang Drive, Singapore 637457

ABSTRACT

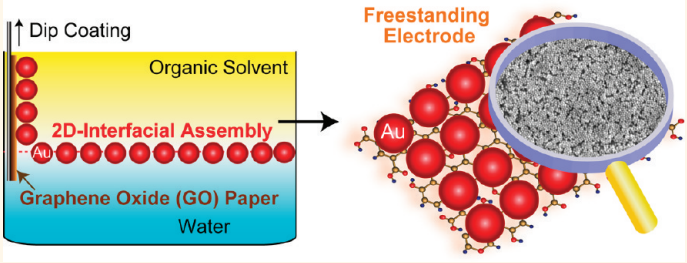

The development of flexible electrodes is of considerable current interest because of the increasing demand for modern electronics, portable medical products, and compact energy devices. We report a modular approach to fabricating high-performance flexible electrodes by structurally integrating 2D-assemblies of nanoparticles with freestanding graphene paper. We have shown that the 2D array of gold nanoparticles at oil–water interfaces can be transferred on freestanding graphene oxide paper, leading to a monolayer of densely packed gold nanoparticles of uniform sizes loaded on graphene oxide paper. One major finding is that the postassembly electrochemical reduction of graphene oxide paper restores the ordered structure and electron-transport properties of graphene, and gives rise to robust and biocompatible freestanding electrodes with outstanding electrocatalytic activities, which have been manifested by the sensitive and selective detection of two model analytes: glucose and hydrogen peroxide (H_2O_2) secreted by live cells. The modular nature of this approach coupled with recent progress in nanocrystal synthesis and surface engineering opens new possibilities to systematically study the dependence of catalytic performance on the structural parameters and chemical compositions of the nanocrystals.

KEYWORDS: flexible electrode · graphene · self-assembly · nanocrystal · electrocatalysis · biosensors

In this article, we report a modular approach to fabricating high-performance flexible electrodes by structurally integrating 2D-assemblies of electrocatalytic nanoparticles with freestanding graphene paper. The development of flexible electrodes is a topic of considerable current interest because of the ever increasing demand for modern electronics, portable medical products, and compact energy devices.[1−7] Hybrid electrodes with functional nanocrystals anchored on carbon substrates are under intense research for a broad spectrum of applications in sensing, energy conversion and storage, and catalysis.[8−12] Among the large family of carbon materials, graphene, consisting of a single-layer of sp^2-hybridized carbon atoms, has emerged as a new class of supporting scaffolds for nanocrystals because of a unique collection of structural and electronic properties such as large surface areas, chemical inertness, and superior electrical conductivity.[13−16] Nanocomposites of graphene and nanocrystals have shown enhanced electron transport and improved activities in catalysis and light harvesting.[17,18] Of particular significance for uses in flexible electrodes, individual graphene nanosheets recently have been assembled into various forms of freestanding paper-like structures with excellent mechanical strength, structural uniformity, and electrical conductivity.[19−24] Increasing evidence has shown that flexible control over the size, morphology, degree of loading, and distribution of the nanocrystals on the substrates is critical for optimizing the performance of the electrodes.[25−28] For instance, in electrocatalytic applications, it is highly desirable to load monodisperse nanocrystals uniformly and in high density to achieve large active surface areas.[29] To be anchored on graphene substrates, nanocrystals currently are either *in situ* synthesized in the presence of graphene or adsorbed on graphene from their colloidal dispersions.[30−33] The functional groups on graphene substrates or attached organic mediators can facilitate the binding of nanocrystals through noncovalent interactions.[34,35]

* Address correspondence to hduan@ntu.edu.sg.

Received for review August 2, 2011 and accepted December 2, 2011.

Published online December 02, 2011
10.1021/nn202930m

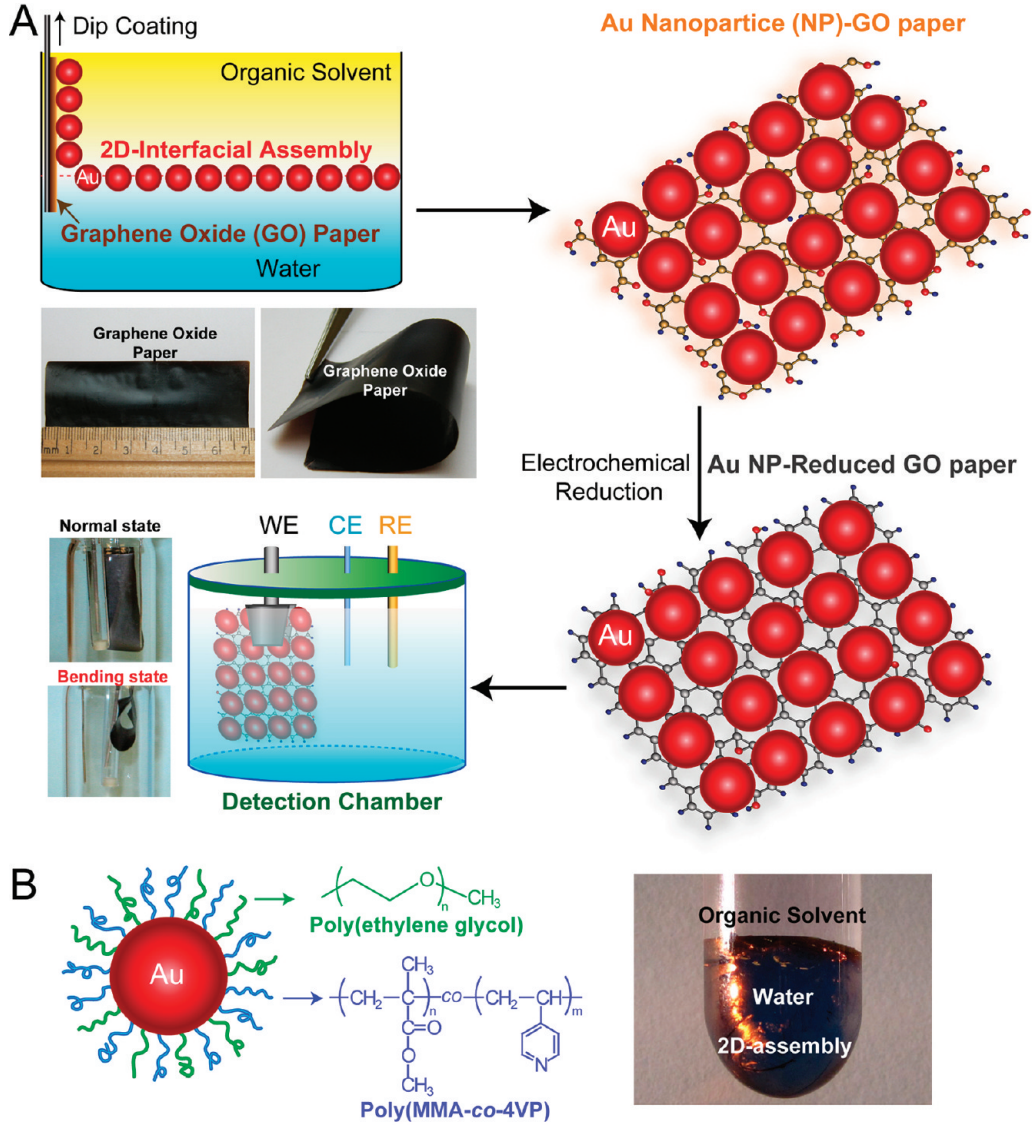

Figure 1. Schematic illustration of the fabrication of freestanding hybrid electrodes from 2D-assembly of gold nanoparticles and graphene oxide paper.

However, *in situ* synthesis of nanocrystals generally does not allow for tailoring the size and morphology of the nanocrystals, and physical adsorption often gives rise to low loading and aggregation of nanocrystals on the substrates.

Recent reports by several groups including us have shown that nanoparticles with rationally designed surface coatings have a tendency to accumulate at the interface of two immiscible liquids, thermodynamically driven by the decrease of total free energy.[36−39] Promoted by the advances in synthesis and surface engineering of well-defined nanocrystals, this strategy has become a widely applicable method to prepare closely packed 2D arrays of metal and semiconductor nanocrystals with controlled sizes and morphologies. In the current proof-of-concept study, we have demonstrated that the use of 2D array of gold nanoparticles at oil−water interfaces and freestanding graphene oxide (GO) paper as the modular building blocks of hybrid electrodes can effectively address the above-mentioned problems encountered in existing methods, leading to a monolayer of densely packed gold nanoparticles of uniform sizes loaded on graphene oxide paper. One interesting finding is that the hydrophilic nature of the GO paper, built-up from exfoliated GO nanosheets through evaporation-assisted assembly, is critical for the successful transfer of the 2D array on the substrates by dip-coating. And the noncovalent interactions between the polymer coating of gold nanoparticles and GO paper also contribute to the robust linking between the two components. More importantly, our results have shown that the postassembly electrochemical reduction of graphene oxide paper restores the ordered structure and electron-transport properties of graphene, and gives rise to biocompatible freestanding electrodes with outstanding

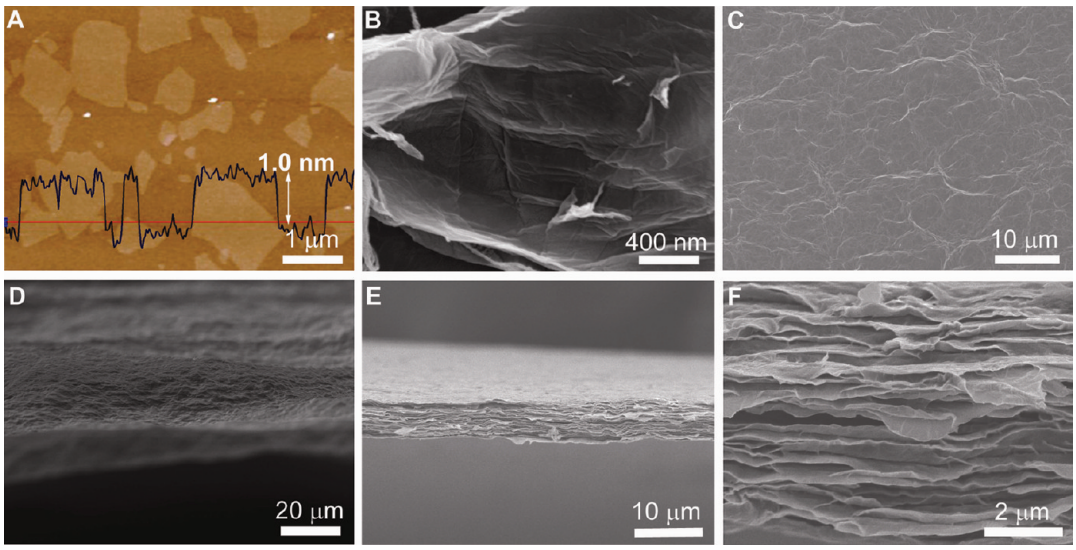

Figure 2. (A) AFM and (B) SEM images of GO sheets. Top (C), tilted (D), and cross-sectional (E, F) view of the as-prepared GO paper.

electrocatalytic activities, which have been manifested by the sensitive and selective detection of two model analytes: glucose and hydrogen peroxide (H_2O_2) secreted by live cells. In comparison with the control electrodes such as reduced GO (rGO) paper and bare gold foil (Au-foil), our flexible electrode leads to greatly enhanced current density and decreased overpotential toward direct electrochemical oxidation/reduction of the electroactive molecules of interests. And the electrode shows identical performances in terms of sensitivity, stability, and response rate even when it is folded, which is of great importance for its utilization in miniaturized and compact devices.

RESULTS AND DISCUSSION

Preparation and Characterization of the Freestanding Hybrid Electrode. As illustrated in Figure 1, the modular scheme toward the hybrid electrodes has three key steps. First, GO paper and 2D-assembly of gold nanoparticles are individually optimized. Second, the 2D-assembly is transferred on the GO paper fixed on a solid substrate through dip-coating. Third, the GO paper coated with the 2D-assembly (Au-GO paper) is electrochemically reduced to yield the hybrid electrode of rGO carrying the closely packed monolayer of gold nanoparticles (Au-rGO paper). The freestanding electrode offers ultimate flexibility for device packaging, and its electrocatalytic activity was tested in three-electrode system using Au-rGO paper as working electrode.

To prepare hydrophilic GO paper, the aqueous dispersion of GO nanosheets, exfoliated from graphite oxide through extensive ultrasonication, was placed in a casting mold made of polytetrafluoroethylene (PTFE). After water was completely removed through slow evaporation at room temperature, freestanding GO paper can be easily peeled off from the low-surface energy PTFE substrate. The height profile in atomic force microscopy (AFM) image (Figure 2A) reveals that the thickness (~1.0 nm) of the GO nanosheets is very close to that of single-layer graphene, suggesting nearly complete exfoliation of the graphite oxide.[40−42] The wrinkled feature of dried graphene nanosheets in scanning electron microscopy (SEM) image (Figure 2B) is indicative of the flexibility of the graphene nanosheets.[42] SEM observation (Figure 2C−F) shows that the GO paper has smooth surface and uniform thickness (~8 μm) throughout the entire cross-section, and the layered structure of stacked graphene nanosheets is clearly distinguishable. The size of the GO paper can be freely adjusted by choosing different-sized casting mold, and the thickness of the paper can also be tailored in the range of 1−30 μm by using different volume of GO dispersion. The 2D array of gold nanocrystals was formed by 14 nm nanocrystals coated with mixed polymer brushes of poly(ethylene glycol) (PEG) and copolymers of methyl methacrylate and 4-vinyl pyridine (PMMAVP) (Figure 1B). The mixed polymer brushes were grafted on the particles through tandem "grafting to" and "grafting from" reactions that we developed recently.[36,43,44] In the mixture of water and chloroform, the gold nanoparticles (Au@PEG/PMMAVP) preferentially stay in the organic phase because of the favorable solubility of the hydrophobic PMMAVP brush in chloroform. As we have demonstrated previously,[36] the addition of hexane, which is a nonsolvent for both PEG and PMMAVP, reduced the affinity of the nanoparticles with the organic phase, and triggered their self-assembly at the oil−water interface to form a close-packed monolayer. The interfacial assembly exhibits the golden-color reflectance

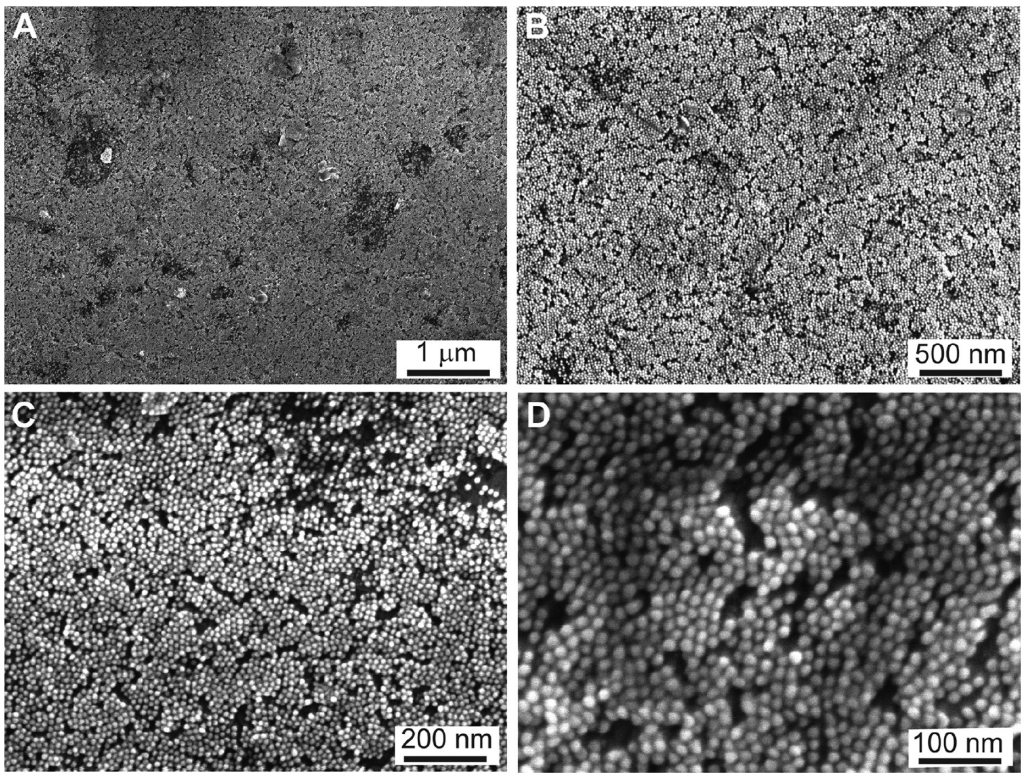

Figure 3. SEM images of 2D-assembly of gold nanoparticles coated on GO paper at different magnifications.

(Figure 1B) due to the strong plasmonic coupling of gold nanoparticles in close proximity.

Figure 3 displays the SEM images of the 2D-assembly of Au@PEG/PMMAVP transferred on the GO paper. It is clear that the gold nanoparticles formed a closely packed monolayer on the surface of GO paper, and the nanoparticle coating is very uniform throughout the entire paper. We have found that the interfacial 2D assembly can only be transferred to substrates that are hydrophilic and wettable by its subphase (water). GO nanosheets have polar functional groups such as hydroxyl, epoxide, and carboxylic acid on the basal plane and edges, which are mostly removed in rGO. Therefore, it is necessary to use hydrophilic GO paper instead of hydrophobic rGO paper as the transferring substrate. We also notice that the 2D assembly of Au@PEG/PMMAVP containing 20% 4-vinyl pyridine (4VP) monomer in the PMMAVP grafts led to better transfer to the GO paper than that formed by the gold nanoparticle coated with polymer brushes containing no 4VP moiety. Presumably, the pyridine groups can form hydrogen bonding with the hydroxyl and carboxylic acids on the GO nanosheets, resulting in stronger affinity between the gold nanoparticles and the GO surfaces. The obtained hybrid electrode exhibits excellent long-term stability, which is confirmed by the chronoamperometric experiments discussed below. Notably, the smooth and uniform surface of graphene paper appears essential for the successful structure integration of the flexible carbon substrate and 2D-assembly of gold nanoparticles. In contrast, loading of the 2D-assembly on buckypaper made of carbon nanotubes led to the discontinued and partially aggregated coating of gold nanoparticles presumably due to the disordered network structure of the buckypaper (see Supporting Information Figure S1).

X-ray photoelectron spectroscopy (XPS) is further employed to quantitatively analyze the degree of the reduction of the GO paper. As shown in Figure 4 A, the C 1s peak of GO shows the presence of four types of carbon bonds: C−C (284.5 eV), C−O (286.6 eV), C═O (288.1 eV), and O−C═O (289.3 eV). Among them, the peak associated with C−O is predominant and the atomic percentage of C/O is 2/1. After the electrochemical reduction, the intensity of the peak associated with C−O greatly reduces, and the C−C peak becomes the predominant peak. The rGO paper exhibits a higher atomic ratio of C/O (7/1), demonstrating that the GO paper was successfully reduced to rGO paper. The stress−strain curve (Figure 4B) of a typical GO paper specimen starts with a straightening stage followed by an elastic deformation. GO paper has a tensile strength of 80 MPa and an ultimate tensile strain of 2.69%, which are further improved to 112.8 MPa and 6.35% in rGO paper. The improved tensile strength and ductility of rGO paper should arise from the stronger interlayer interaction of rGO nanosheets after the oxygen-containing groups are removed in the electrochemical reduction. Our results are also in line with previous reports, showing that GO and rGO paper outperform

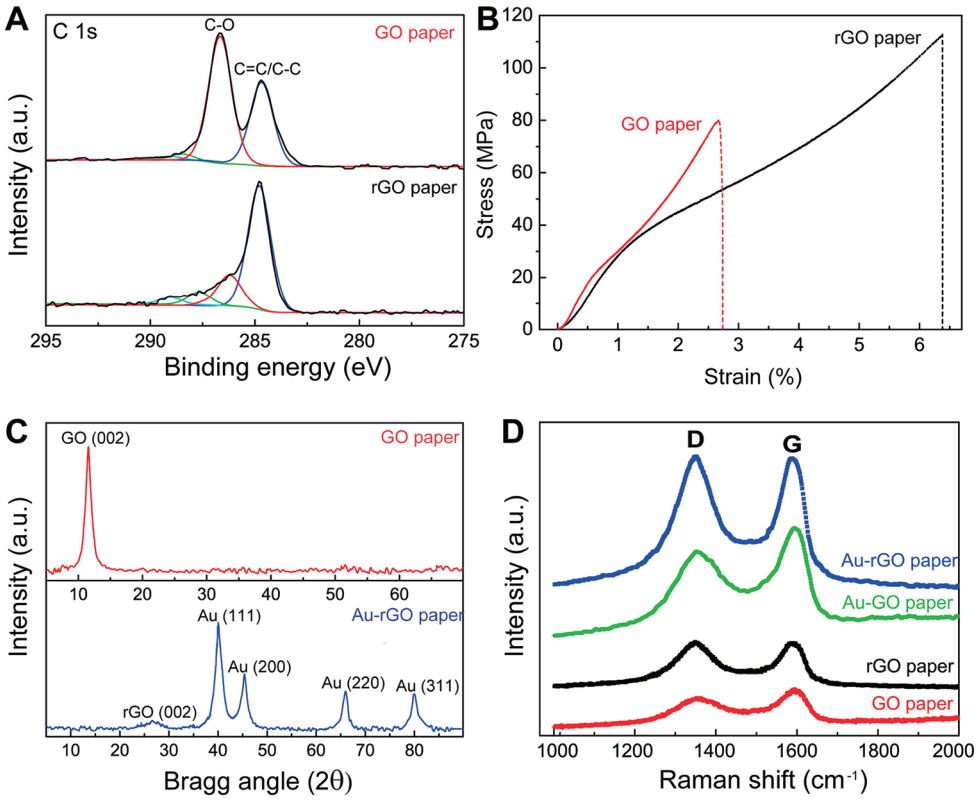

Figure 4. (A) XPS curves fit of C 1s spectra of GO and rGO papers. (B) Stress–strain curves of GO and rGO paper. (C) XRD patterns of GO and Au-rGO papers. (D) Raman spectra of GO, rGO, Au-GO, and Au-rGO papers.

conventional flexible carbon substrates such as graphite foils and bucky paper in mechanical strength.[19−21]

The typical X-ray diffraction (XRD) patterns of the GO paper and Au-rGO paper are shown in Figure 4B. A narrow diffraction peak (2θ = 10.4°) is present for GO paper, corresponding to a layer-to-layer distance (*d*-spacing) of about 0.85 nm. The increased interlayer spacing (>0.6 nm) of GO is due to the intercalated water molecules between neighboring GO layers.[21] The weak and broad peak at 26.6° in Au-rGO paper corresponds to a *d*-spacing of 0.34 nm, which suggests the elimination of the structural water on the rGO sheets.[45] The four peaks at 38.5°, 43.9°, 64.7°, and 78.6° are related to (111), (200), (220), and (311) planes of face-centered-cubic (fcc) Au (JCPDS 04-0784). The peak corresponding to the (111) plane is more intense than the others, indicating that the (111) plane is the dominating orientation. Raman measurements (Figure 4C) were also performed to determine the microstructure of as-prepared paper-like GO, rGO, Au-GO, and Au-rGO samples. GO paper displays two prominent peaks at 1355 and 1595 cm^{-1}, corresponding to the well-documented D and G bands, respectively. In rGO paper, these two peaks remain at the same position. However, the intensity ratio of the two peaks (I_D/I_G) increases in comparison with that of the GO paper, confirming that ordered structure is partially restored in rGO after the electrochemical reduction.[41,42] One interesting finding is that the coating of the 2D assembly of gold nanoparticles leads to about 3-fold enhancement of the Raman signal from GO and rGO. Surface-enhanced Raman scattering (SERS) of small molecules on the surface of colloidal gold nanoparticles and gold substrate is well-documented, and the SERS of graphene by gold nanostructures has also been reported.[45,46] The enhanced electromagnetic field surrounding the 2D assembly is expected to only enhance the Raman signal of a few layer of graphene next to the assembly. Considering that the paper consists of thousand layers of graphene sheets, the actual enhancement factor should be much greater than 3-fold, detected from the entire paper. Taken together, the Au-rGO paper electrode with superior structural integrity has been successfully fabricated in the modular approach.

Electrocatalytic Activities of the Hybrid Electrode. $[Fe(CN)_6]^{3-/4-}$ redox probe was first employed to investigate the intrinsic electrochemical behavior of Au-rGO paper electrode along with control electrodes including GO paper, rGO paper, and bare Au-foil with the same dimension and similar thickness. The results of electrochemical impedance spectroscopy (EIS) of different electrodes are summarized in Figure 5A. Insulating GO paper exhibits huge Faradic charge transfer resistance (R_{ct}), which reduces to 197 Ω in rGO paper because of the restoration of a graphitic network of sp^2 bonds. Interestingly, introducing the 2D assembly of gold nanoparticles on the rGO paper led to a further decrease of R_{ct} to 95 Ω, which is only slightly larger than that (72 Ω) of the Au foil. Cyclic voltammetry (CV)

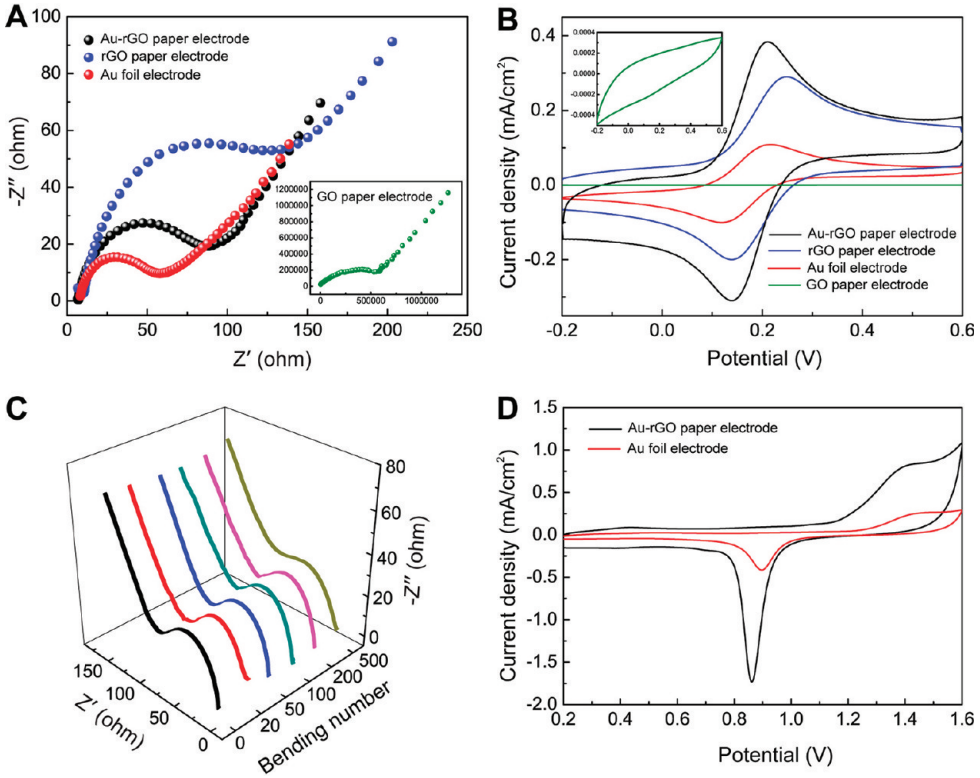

Figure 5. Nyquist plots (A) and CV curves (B) of Au-rGO paper, rGO paper, Au foil and GO paper electrodes in 1.0 mM $K_3Fe(CN)_6$ + 1.0 mM $K_4Fe(CN)_6$. The insets are the CV curve and Nyquist plots of the GO paper. (C) EIS curves of Au-rGO paper electrode after repetitive bending. Supporting electrolyte, 0.1 M KCl; scan rate, 10 mV s^{-1} (for CV); frequency range, 0.1 Hz−10^5 Hz (for EIS). (D) CV curves of Au-rGO paper and Au foil electrodes. Supporting electrolyte, 0.5 M H_2SO_4 saturated with nitrogen gas; scan rate, 10 mV s^{-1}.

measurements (Figure 5B) show that no redox peaks are found on the GO paper electrode, indicating that the insulating GO greatly inhibits the heterogeneous electron transfer between the electrode and the redox species in solution. A pair of quasi-reversible one-electron redox peak is observed on bare Au-foil, rGO, and Au-rGO paper electrodes. However, the Au-rGO electrode exhibits dramatically enhanced peak current (i_p) and reduced peak potential separation (ΔE_p) in comparison with other control electrodes, indicative of enhanced electrochemical activities. The active surface areas of the electrodes are estimated according to the slope of the i_p versus $v^{1/2}$ plot, based on the Randles-Sevcik equation, $i_p = 269n^{3/2}AD^{1/2}v^{1/2}c$, the results are 0.85, 1.89, and 3.05 cm^2 (average of six measurements) for Au foil, rGO, and Au-rGO paper electrodes, respectively. According to the following equation: $R_{ct} = (RT/(n^2F^2Ak^0))\ (1/(C_O^{(1-\alpha)}C_R^{\alpha}))$,[47] where the electron transfer coefficient (α) is 0.5 for the heterogeneous process, and A is the active surface area of the electrodes, the standard electron transfer constants (k^0) of rGO and Au-rGO papers electrodes are 0.98×10^{-3} and 1.30×10^{-3} cm s^{-1}, respectively. Collectively, these results suggest that Au-rGO paper exhibits more effective electron transfer and superior electrochemical activity, which should originate from both of the improved electrical conductivity of Au-rGO paper and the substantially greater active surface area of the 2D-assembly of 14 nm gold nanoparticles than the bulky Au-foil electrode. Our results demonstrate that the amphiphilic polymer coating of the gold nanoparticles do not inhibit the electron transfer between the nanoparticles and the rGO paper substrate. Similar electron transfer between surface-passivated nanoparticles and the electrode surfaces has been reported previously in self-assembled monolayer capped nanoparticles,[48,49] or by incorporating polyelectrolyte multiple layers between nanoparticles and the substrate.[50] It is believed that electron tunneling should be the main factor leading to the observed electron transfer, although a layer of insulating coating is present between the nanoparticles and the electrode substrate. The closely packed gold nanoparticles with a large specific surface area can serve as tiny conduction centers to facilitate the electron transfer between the $[Fe(CN)_6]^{3-/4-}$ probe and the rGO substrate.

Next, we investigated the impact of physical deformation and mechanical stress on the electrochemical performance of Au-rGO paper. Our results have demonstrated that 500 times of repetitive inward 180° bending did not affect the resistance behavior of Au-rGO paper measured in the redox reaction of $Fe(CN)_6]^{3-/4-}$ (Figure 5C). The influence of the bending-induced mechanical stress on the CV response of the Au-rGO paper was also examined (see Supporting Information Figure S2). The results show that the change in the CV response is less than 5% after

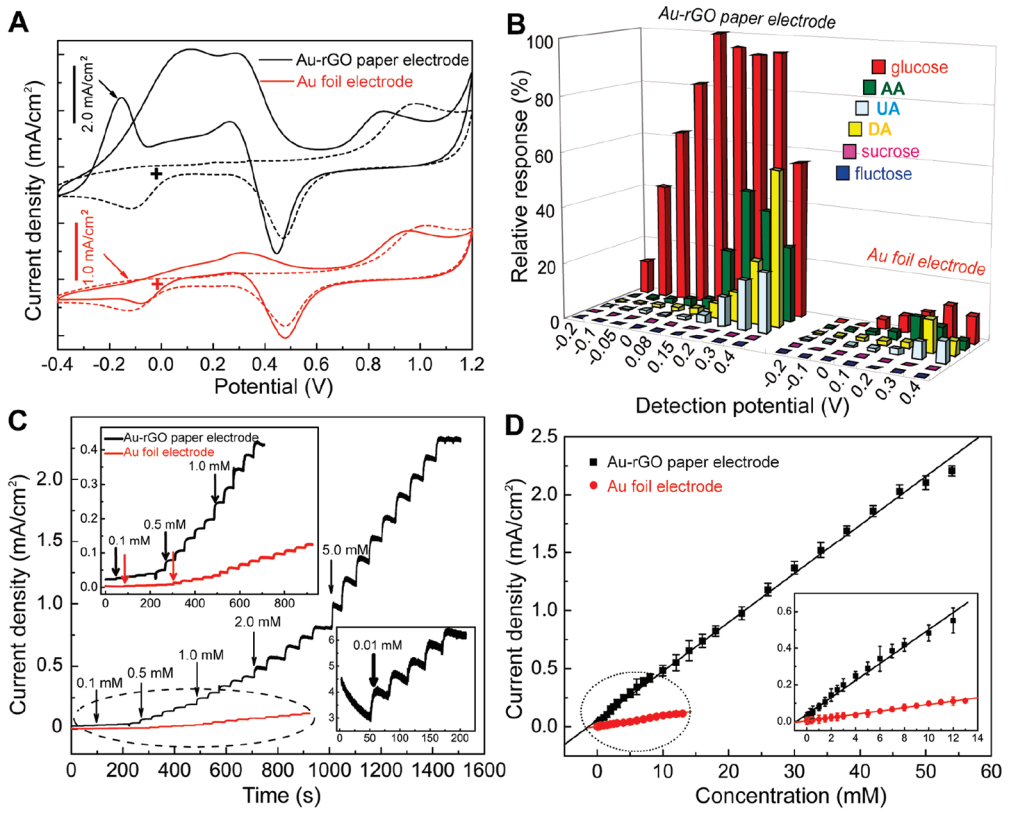

Figure 6. (A) CV curves of Au-rGO paper electrode (top) and Au foil electrode (bottom) in 0.1 M PBS (pH 7.4) saturated with nitrogen gas in the absence (dashed line) and in the presence of 10 mM glucose (solid line). Scan rate: 10 mV s^{-1}. (B) Amperometric responses of Au-rGO paper and Au foil electrodes to the analytes of interest at different detection potential. (C) Typical amperometric response of Au-rGO paper electrode and Au foil electrode to the successive addition of 0.1, 0.5, 1.0, 2.0, and 4.0 mM glucose in PBS buffer (pH 7.4) under magnetic stirring; insets show the amperometric response of Au-rGO paper and Au foil electrodes at a lower concentration detected. (D) Corresponding calibration curves. Applied potential: 0.08 V for Au-rGO paper electrode, 0.3 V for Au foil electrode.

the Au-rGO paper is maintained at inward 180° bending for 196 h or bent for 500 times, suggesting the remarkable mechanical stability of the flexible paper electrode.

The CV curves (Figure 5C) of Au-rGO paper and bare Au-foil electrodes in 0.5 M H_2SO_4 display the characteristic feature of the redox reaction of gold, and Au-rGO paper electrode shows much higher current density associated with gold oxide formation/reduction events than that of Au-foil electrode. This evidence further confirms that the surface of the gold nanoparticles is electrochemically active. The active surface areas of Au-rGO paper and Au-foil are estimated by integrating the gold reduction peak corrected for the baseline. The charge required for a monolayer of gold oxides is 390 μC cm^{-2}.[49] The calculated surface area of Au-rGO paper is 3.79 cm^2 (average of six measurements), which is over six times of that (0.60 cm^2) of Au-foil. The Au-rGO paper has a roughness factor (RF) of 7.8, which is defined as the ratio of the active surface area over the geometrical area. The large RF of Au-rGO paper is indicative of its excellent catalytic activity in selectively enhancing the faradic current of kinetically controlled sluggish reactions.

To assess the electrocatalytic activity of the Au-rGO paper electrode, we tested its performance toward the oxidation of glucose, which is a marker for the diagnosis of diabetes. Figure 6A depicts the CVs of Au-rGO paper electrode and different control electrodes in the absence and presence of 10 mM glucose in N_2-saturated PBS (pH 7.4). The absence of oxidation currents of glucose on both rGO and GO papers (see Supporting Information, Figure S3) indicates that the graphene-based paper electrodes alone have negligible electrocatalytic activity toward glucose oxidation. Multiple peaks associated with the oxidation of glucose and the resultant intermediates as well as the redox of Au/AuOH are found in the positive and negative scans on Au-rGO paper and Au-foil. In contrast to Au-foil electrode, the hybrid paper electrode shows remarkably higher current densities at lower onset potentials for glucose oxidation, which are highly desirable characters for the use of this flexible platform in electrochemical biosensing. Particularly, in amperometric detection, the relative negative potential (0.08 V) of glucose oxidation on Au-rGO paper can effectively eliminate the interference of the common electroactive species such as ascorbic acid (AA), dopamine (DA), and uric acid (UA) that normally coexist with glucose in biological systems and food samples,

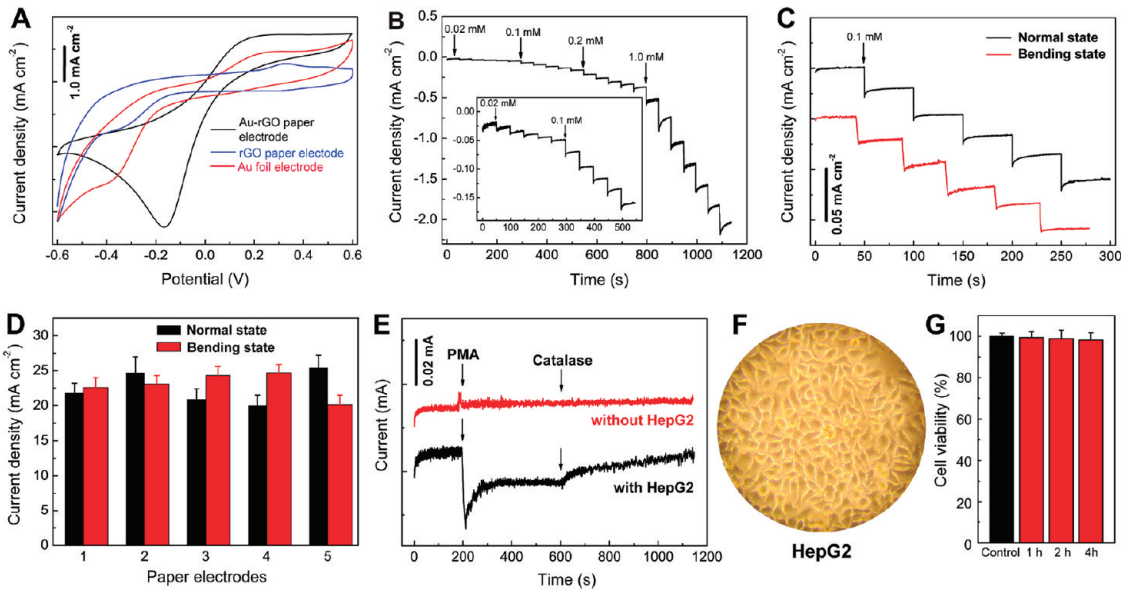

Figure 7. (A) CV curves of Au-rGO paper and Au foil electrodes in 0.1 M PBS (pH 7.4) in the presence of 5 mM H_2O_2. Scan rate: 50 mV s^{-1}. (B) Typical amperometric response of Au-rGO paper electrode to successive addition of 0.02, 0.1, 0.2, and 1.0 mM H_2O_2 in a stirring PBS; the inset shows the amperometric response to successive addition of 5 and 10 μM H_2O_2. (C) Typical amperometric response and the comparison of Au-rGO paper electrode to successive addition of 0.1 mM H_2O_2 in a stirring PBS under normal test and bending conditions. (D) Corresponding histograms of panel C. (E) Amperometric responses of the Au-rGO paper electrode in 0.1 M PBS (pH 7.4) with the addition of 0.1 mM PMA and 300 U mL^{-1} catalase in the absence and presence of HepG2 cells. (F) Bright-field image of HepG2 cells used in the *in vitro* tests. (G) Quantitative cell viability results.

since the oxidation of these species usually happens in the potential more than 0.3 V in the PBS buffer (pH 7.4). Figure 6B compares the amperometric response of glucose and all the potential interfering substances at the Au-rGO paper and Au foil electrodes. Common saccharides such as sucrose and fructose are not electroactive and do not cause any interference for the detection of glucose. Obviously, when the applied detection potential shifts below 0.1 V, the electrochemical response of AA, DA, and UA on the Au-rGO paper electrode decreases dramatically, and their interference becomes negligible. In contrast, the interference from AA, DA, and UA is a serious problem for the Au foil electrode, as its maximum current response occurs at about 0.3 V. Figure 6C shows the typical amperometric responses of the Au-rGO paper and Au foil upon the successive injection of glucose into the PBS solution (pH 7.4). Upon each addition of glucose, the response of the Au-rGO paper electrode based-sensor rapidly reaches 95% of the steady-state value within 3 s. A good linear dependence on the glucose concentration in the range of 0.01−46 mM was achieved, with a sensitivity of 52.36 μA cm^{-2} mM^{-1} and a detection limit down to 5 μM at a signal-to-noise (S/N) ratio of 3 (Figure 6D). For the Au foil electrode, the linear range is only from 0.1 to 11 mM with a sensitivity of 9.01 μA cm^{-2} mM^{-1} and a detection limit of 50 μM. Reproducibility and stability of the electrode are also important parameters to evaluate the performance of an electrochemical biosensor. We have found that the results of 10 individual measurements of 10.0 mM glucose using Au-rGO paper have a relative standard deviation of 2.36%. The paper electrode also exhibits excellent short-term and long-term stability: the peak current for glucose oxidation retains 96.8% of its initial value after 200 successive cycles; the catalytic potential is almost unchanged, and the catalytic current was still over 90% of the initial value at 60 days postpreparation.

To further examine the biocompatibility and performance of the Au-rGO paper electrode in living systems, we have used it for real-time tracking the secretion of H_2O_2 by live cells. H_2O_2 is the most stable reactive oxygen species, which are known to serve as messengers in a number of regular cellular functions, and also play important roles in undesired oxidative stress, aging and pathological process such as cancer, cardiovascular disease and neurological disorder.[51] Figure 7A shows the CV curves of Au-rGO paper, Au-foil and rGO paper electrodes in PBS (pH 7.4) toward H_2O_2 reduction. In contrast to the poor response of Au-foil and rGO paper electrodes, Au-rGO paper electrode leads to much larger current density and lower overpotential in the direct redox of H_2O_2. Therefore, it can be expected that gold nanoparticles rather than the rGO paper play a major role in the electrocatalytic activity observed in the Au-rGO electrode. The amperometric responses (Figure 7B and C) of the Au-rGO paper electrode to the successive additions to H_2O_2 show that the rapidly equilibrated current is proportional to the concentration of H_2O_2 in the range of 0.005−8.6 mM, with a sensitivity of 236.8 μA cm^{-2} mM^{-1}. And the detection limit is down

to 2 μM based on S/*N* = 3 (see Supporting Information Figure S4 for the calibration curve). This novel type of flexible biosensor has outstanding analytical performance in sensing H_2O_2, which make it useful in different detection systems for *in vitro* and *in vivo* H_2O_2 detection. Our freestanding paper electrode offers the unique advantage of flexible processing, which is supported by its identical amperometric responses (Figure 7D) no matter when it stays upright or folded. Next, we used the Au-rGO electrode for tracking live-cell H_2O_2 secretion. HepG2 cells of 80% confluency were maintained in 0.1 M PBS (pH 7.4), and were stimulated to release H_2O_2 by phorbol 12-myristate-13-acetate (PMA). As shown in Figure 7E, a considerable cathodic current density of 1.75 μA cm^{-2} is observed upon the addition of PMA for HepG2, followed by a gradual decrease of current, and stays stable at 0.65 μA cm^{-2} after 90 s. Interestingly, addition of catalase, a scavenger of H_2O_2, results in a sudden drop of current response, which further decreases down to the level of background signal afterward. Control wells containing no HepG2 cells do not generate any signal response to the addition of PMA or catalase. The cells incubated with the Au-rGO paper electrode for over 4 h are very healthy (Figure 7F), and maintain over 95% viability after 4 h incubation with the paper electrode (Figure 7G). The fast and sensitive response of the Au-rGO paper electrode to low concentrations of H_2O_2 secreted by live cells and its biocompatibility promise its potential uses to detect oxidative stress that cancer cells in the hypoxia state often experience.

CONCLUSIONS

We have developed a new type of high-performance flexible hybrid electrodes by taking advantage of two modular platforms: freestanding graphene paper and closely packed 2D-assembly of catalytic nanocrystals with well-defined surface coating. The freestanding paper electrode, integrating the structural and electrical properties of graphene papers and the extremely large active surface areas of the nanocrystals, has demonstrated extraordinary electrocatalytic activities in electrochemical sensing of glucose and live-cell-secreted H_2O_2. The modular nature of this approach coupled with recent progress in nanocrystal synthesis and surface engineering opens new possibilities to systematically study the dependence of catalytic performance on the structural parameters and chemical compositions of the nanocrystals. We envision that the broader application of this strategy will contribute to the development of the next generation of flexible bionanoelectronics and energy storage devices.

EXPERIMENTAL SECTION

Reagents were obtained from Sigma-Aldrich unless specified otherwise. Methoxy-poly(ethylene glycol)-thiol (PEG) with a molecular weight of 5000 Da was purchased from Laysan Bio, Inc. Chloroauric acid was obtained from Alfa Aesar. For electrochemical experiments, the working solutions were prepared by diluting the stock solution with phosphate buffer solution (PBS) and water. All other chemicals used were of analytical reagent grade.

CV, EIS, and chronoamperometric experiments were performed with a CHI 660 D electrochemical workstation (CH Instrument Company). A conventional three-electrode system was adopted. The working electrodes were the graphene paper (1 cm $\times$0.5 cm) and commercial smooth Au foil with the same dimension. The auxiliary and reference electrodes were Pt wire and Ag/AgCl, respectively. The scanning electron microscopy images were obtained on a FESEM instrument (JSM-6700F, Japan). Atomic force microscopy measurements were conducted on a MFP-3D microscope (Asylum research). X-ray photoelectron spectroscopy (XPS) measurements were performed on a Kratos-Axis spectrometer with monochromatic Al Kα (1486.71 eV) X-ray radiation (15 kV and 10 mA) and hemispherical electron energy analyzer. X-ray diffraction (XRD) data were recorded with an X-ray diffractometer Bruker AXS D8 using Cu Kα radiation (40 kV, 200 mA) with a Ni filter. Raman spectra were acquired with a micro-Raman spectrometer (Reinshaw Raman Scope RM3000) in the backscattering configuration using an Ar-ion laser with wavelength 514.5 nm. All measurements were conducted at room temperature.

Gold nanoparticles of 14 nm were synthesized using standard citrate reduction. Gold nanoparticles coated with PEG and PMMAVP were synthesized in two steps: first, PEG and an atom transfer radical polymerization (ATRP) initiator 2,2′-dithiobis[1-(2-bromo-2-methyl-propionyloxy)] ethane (DTBE) were coated on the nanoparticle through ligand exchange; second, the coated nanoparticles were used to initiate the ATRP of MMA and 4VP monomers.[43] In the two-phase system of chloroform and water, the nanoparticles stayed in chloroform. Hexane (hexane/chloroform = 4:1, v/v) was added and the mixture was gently shaken to induce the interfacial assembly of the nanoparticles.[36]

The graphite oxide (GO) was synthesized from synthetic graphite powder based on a modified Hummers method. Then the exfoliation of GO was achieved by ultrasonication of the dispersion for 2 h. GO paper was prepared by evaporation-assisted self-assembly process. In details, the aqueous dispersion of GO nanosheets was placed in a casting mold made of polytetrafluoroethylene (PTFE). After water was completely removed through slow evaporation at room temperature, freestanding GO paper was peeled off from the low-surface energy PTFE substrate, and then was processed for further uses. The 2D-assembly of amphiphilic gold nanoparticles was prepared according to our recent work,[36,40,44] and then transferred on the surface of GO paper by dip-coating. Then the papers were cut into small pieces of specific dimensions as electrodes for electrochemical reduction.[41−43] The electrochemical reduction of GO paper and Au-GO paper was performed at a constant potential (−1.5 V *vs* Ag/AgCl) in 0.1 M PBS (pH = 7.0). A piece of Au foil was used to connect the GO paper and the clips, and the temperature of the solution was maintained at 80 °C in order to accelerate the reaction rate. All the modified electrodes were washed carefully with redistilled water and then dried at room temperature.

HepG2 cells were obtained from ATCC (USA), and the cells were maintained in Delbecco's modified minimum essential medium

at 37 °C (5% CO_2) and subcultured every 3 days. To detect the secretion of H_2O_2 by live cell, the cells were grown in a 24-well plate to 80% confluency, and a conventional three-electrode system with the graphene paper (1 cm × 0.5 cm) as the working electrode was adopted for the electrochemical experiments (As shown in Figure 1). Cytotoxicity of the Au-rGO paper electrode was evaluated using a standard cell counting Kit-8 (CCK-8) assay in a 96-well plate.[52] One piece of Au-rGO paper was added into every well tested and incubated with the HepG2 cells for 1−4 h. Afterward, CCK-8 solutions were added to each tested wells, and the absorbance of every well at 450 nm was measured using a microplate reader after 4 h incubation. The cell viability was calculated based on the ratio of the absorbance of the sample well to that of the control cell and expressed as a percentage.

Acknowledgment. H.D. thanks the program of Nanyang Assistant Professorship for financial support. This work is partly supported by AcRF grants (ARC25/08) from Ministry of Education (Singapore) to R.X.

Supporting Information Available: Additional figures as described in the text. This material is available free of charge *via* the Internet at http://pubs.acs.org.

REFERENCES AND NOTES

1. Lu, X. M.; Xia, Y. N. Electronic Materials: Buckling down for Flexible Electronics. *Nat. Nanotechnol.* **2006**, *1*, 163–164.
2. Pushparaj, V. L.; Shaijumon, M. M.; Kumar, A.; Murugesan, S.; Ci, L.; Vajtai, R.; Linhardt, R. J.; Nalamasu, O.; Ajayan, P. M. Flexible Energy Storage Devices Based on Nanocomposite Paper. *Proc. Natl. Acad. Sci. U.S.A.* **2007**, *104*, 13574–13577.
3. Nishide, H.; Oyaizu, K. Toward Flexible Batteries. *Science* **2008**, *319*, 737–738.
4. Cheung, W.; Chiu, P. L.; Parajuli, R. R.; Ma, Y.; Ali, S. R.; He, H. Fabrication of High Performance Conducting Polymer Nanocomposites for Biosensors and Flexible Electronics: Summary of the Multiple Roles of DNA Dispersed and Functionalized Single Walled Carbon Nanotubes. *J. Mater. Chem.* **2009**, *19*, 6465–6480.
5. Sekitani, T.; Yokota, T.; Zschieschang, U.; Klauk, H.; Bauer, S.; Takeuchi, K.; Takamiya, M.; Sakurai, T.; Someya, T. Organic Nonvolatile Memory Transistors for Flexible Sensor Arrays. *Science* **2009**, *326*, 1516–1519.
6. Chuang, M. C.; Yang, Y. L.; Tseng, T. F.; Chou, T.; Lou, S. L.; Wang, J. Flexible Thick-Film Glucose Biosensor: Influence of Mechanical Bending on the Performance. *Talanta* **2010**, *81*, 15–19.
7. Brezesinski, T.; Wang, J.; Tolbert, S. H.; Dunn, B. Ordered Mesoporous α-MoO_3 with Iso-oriented Nanocrystalline Walls for Thin-Film Pseudocapacitors. *Nat. Mater.* **2010**, *9*, 146–151.
8. Khalap, V. R.; Sheps, T.; Kane, A. A.; Collins, P. G. Hydrogen Sensing and Sensitivity of Palladium-Decorated Single-Walled Carbon Nanotubes with Defects. *Nano Lett.* **2010**, *10*, 896–901.
9. Sanles-Sobrido, M.; Correa-Duarte, M. A.; Carregal-Romero, S.; Rodríguez-González, B.; Álvarez-Puebla, R. A.; Hervés, P.; Liz-Marzán, L. M. Highly Catalytic Single-Crystal Dendritic Pt Nanostructures Supported on Carbon Nanotubes. *Chem. Mater.* **2009**, *21*, 1531–1535.
10. Liao, S.; Holmes, K. A.; Tsaprailis, H.; Briss, V. I. High Performance PtRulr Catalysts Supported on Carbon Nanotubes for the Anodic Oxidation of Methanol. *J. Am. Chem. Soc.* **2006**, *128*, 3504–3505.
11. Hou, Y.; Cheng, Y. W.; Hobson, T.; Liu, J. Design and Synthesis of Hierarchical MnO_2 Nanospheres/Carbon Nanotubes/Conducting Polymer Ternary Composite for High Performance Electrochemical Electrodes. *Nano Lett.* **2010**, *10*, 2727–2733.
12. Zanolli, Z.; Leghrib, R.; Felten, A.; Pireaux, J. J.; Llobet, E.; Charlier, J. C. Gas Sensing with Au-Decorated Carbon Nanotubes. *ACS Nano* **2011**, *5*, 4592–4599.
13. Novoselov, K. S.; Geim, A. K.; Morozov, S. V.; Jiang, D.; Zhang, Y.; Dubonos, S. V.; Grigorieva, I. V.; Firsov, A. A. Electric Field Effect in Atomically Thin Carbon Films. *Science* **2004**, *306*, 666–669.
14. Geim, A. K.; Novoselov, K. S. The Rise of Graphene. *Nat. Mater.* **2007**, *6*, 183–191.
15. Stankovich, S.; Dikin, D. A.; Dommett, G. H. B.; Kohlhaas, K. M.; Zimney, E. J.; Stach, E. A.; Piner, R. D.; Nguyen, S. T.; Ruoff, R. D. Graphene-Based Composite Materials. *Nature* **2006**, *442*, 282–286.
16. Geim, A. K. Graphene: Status and Prospects. *Science* **2009**, *324*, 1530–1534.
17. Guo, S.; Dong, S.; Wang, E. Three-Dimensional Pt-on-Pd Bimetallic Nanodendrites Supported on Graphene Nanosheet: Facile Synthesis and Used as an Advanced Nanoelectrocatalyst for Methanol Oxidation. *ACS Nano* **2010**, *4*, 547–555.
18. Yoo, E. J.; Okata, T.; Akita, T.; Kohyama, M.; Nakamura, J.; Honma, I. Enhanced Electrocatalytic Activity of Pt Subnanoclusters on Graphene Nanosheet Surface. *Nano Lett.* **2009**, *9*, 2255–2259.
19. Chen, C.; Yang, Q. H.; Yang, Y.; Lv, W.; Wen, Y.; Hou, P. X.; Wang, M.; Cheng, H. M. Self-Assembled Free-Standing Graphite Oxide Membrane. *Adv. Mater.* **2009**, *21*, 3007–3011.
20. Chen, H.; Müller, M. B.; Gilmore, K. J.; Wallace, G. G.; Li, D. Mechanically Strong, Electrically Conductive, and Biocompatible Graphene Paper. *Adv. Mater.* **2008**, *20*, 3557–3561.
21. Dikin, D. A.; Stankovich, S.; Zimney, E. J.; Piner, R. D.; Dommett, G. H. B.; Evmenenko, G.; Nguyen, S. T.; Ruoff, R. S. Preparation and Characterization of Graphene Oxide Paper. *Nature* **2007**, *448*, 457–460.
22. Chen, Z.; Ren, W.; Gao, L.; Liu, B.; Pei, S.; Cheng, H. M. Three-Dimensional Flexible and Conductive Interconnected Graphene Networks Grown by Chemical Vapour Deposition. *Nat. Mater.* **2011**, *10*, 424–428.
23. Wang, D. W.; Li, F.; Zhao, J.; Ren, W.; Chen, Z. G.; Tan, J.; Wu, Z. S.; Gentle, I.; Lu, G. Q.; Cheng, H. M. Fabrication of Graphene/Polyaniline Composite Paper *via in Situ* Anodic Electropolymerization for High-Performance Flexible Electrode. *ACS Nano* **2009**, *3*, 1745–1752.
24. Choi, B. G.; Park, H.; Park, T. J.; Yang, M. H.; Kim, J. S.; Jang, S. Y.; Heo, N. S.; Lee, S. Y.; Kong, J.; Hong, W. H. Solution Chemistry of Self-Assembled Graphene Nanohybrids for High-Performance Flexible Biosensors. *ACS Nano* **2010**, *4*, 2910–2918.
25. Guo, S.; Dong, S.; Wang, E. Three-Dimensional Pt-on-Pd Bimetallic Nanodendrites Supported on Graphene Nanosheet: Facile Synthesis and Used as an Advanced Nanoelectrocatalyst for Methanol Oxidation. *ACS Nano* **2010**, *4*, 547–555.
26. Guo, S.; Wen, D.; Zhai, Y.; Dong, S.; Wang, E. Platinum Nanoparticle Ensemble-on-Graphene Hybrid Nanosheet: One-Pot, Rapid Synthesis, and Used as New Electrode Material for Electrochemical Sensing. *ACS Nano* **2010**, *4*, 3959–3968.
27. Campuzano, S.; Wang, J. Nanobioelectroanalysis Based on Carbon/Inorganic Hybrid Nanoarchitectures. *Electroanalysis* **2011**, *23*, 1289–1300.
28. Manna, L.; Scher, E. C.; Alivisatos, A. P. Synthesis of Soluble and Processable Rod-, Arrow-, Teardrop-, and Tetrapod-Shaped CdSe Nanocrystals. *J. Am. Chem. Soc.* **2000**, *122*, 12700–12706.
29. Yu, A.; Liang, Z.; Cho, J.; Caruso, F. Nanostructured Electrochemical Sensor Based on Dense Gold Nanoparticle Film. *Nano Lett.* **2003**, *3*, 1203–1207.
30. Kamat, P. V. Graphene-Based Nanoarchitectures. Anchoring Semiconductor and Metal Nanoparticles on a Two-Dimensional Carbon Support. *J. Phys. Chem. Lett.* **2010**, *1*, 520–527.
31. Wang, H.; Cui, L. F.; Yang, Y.; Casalongue, H. S.; Robinson, J. T.; Liang, Y.; Cui, Y.; Dai, H. Mn_3O_4-Graphene Hybrid as a High-Capacity Anode Material for Lithium Ion Batteries. *J. Am. Chem. Soc.* **2010**, *132*, 13978–13980.
32. Vinodgopal, K.; Neppolian, B.; Lightcap, I. V.; Grieser, F.; Ashokkumar, M.; Kamat, P. V. Sonolytic Design of Graphene-Au Nanocomposites. Simultaneous and Sequential Reduction

of Graphene Oxide and Au(III). *J. Phys. Chem. Lett.* **2010**, *1*, 1987–1993.
33. Zhang, S.; Shao, Y.; Liao, H.; Liu, J.; Aksay, I. A.; Yin, G.; Lin, Y. Graphene Decorated with PtAu Alloy Nanoparticles: Facile Synthesis and Promising Application for Formic Acid Oxidation. *Chem. Mater.* **2011**, *23*, 1079–1081.
34. Liu, J.; Fu, S. H.; Yuan, B.; Li, Y. L.; Deng, Z. X. Toward a Universal "Adhesive Nanosheet" for the Assembly of Multiple Nanoparticles Based on a Protein-Induced Reduction/Decoration of Graphene Oxide. *J. Am. Chem. Soc.* **2010**, *132*, 7279–7281.
35. Goncalves, G.; Marques, P. A. A. P.; Granadeiro, C. M.; Nogueira, H. I. S.; Singh, M. K.; Gracio, J. Surface Modification of Graphene Nanosheets with Gold Nanoparticles: The Role of Oxygen Moieties at Graphene Surface on Gold Nucleation and Growth. *Chem. Mater.* **2009**, *21*, 4796–4802.
36. Cheng, L.; Liu, A.; Peng, S.; Duan, H. W. Responsive Plasmonic Assemblies of Amphiphilic Nanocrystals at Oil–Water Interfaces. *ACS Nano* **2010**, *4*, 6098–6104.
37. Lin, Y.; Skaff, H.; Emrick, T.; Dinsmore, A. D.; Russell, T. P. Nanoparticle Assembly and Transport at Liquid–Liquid Interfaces. *Science* **2003**, *299*, 226–229.
38. Duan, H. W.; Wang, D. Y.; Sobal, N. S.; Giersig, M.; Kurth, D. G.; Möhwald, H. Magnetic Colloidosomes Derived from Nanoparticle Interfacial Self-Assembly. *Nano Lett.* **2005**, *5*, 949–952.
39. Arumugam, P.; Patra, D.; Samanta, B.; Agasti, S. S.; Subramani, C.; Rotello, V. M. Self-Assembly and Cross-Linking of FePt Nanoparticles at Planar and Colloidal Liquid–Liquid Interfaces. *J. Am. Chem. Soc.* **2008**, *130*, 10046–10047.
40. Guo, H. L.; Wang, X. F.; Qian, Q. Y.; Wang, F. B.; Xia, X. H. A Green Approach to the Synthesis of Graphene Nanosheets. *ACS Nano* **2009**, *3*, 2653–2659.
41. Gao, H.; Xiao, F.; Ching, C. B.; Duan, H. W. One-Step Electrochemical Synthesis of PtNi Nanoparticle–Graphene Nanocomposites for Nonenzymatic Amperometric Glucose Detection. *ACS Appl. Mater. Interfaces* **2011**, *3*, 3049–3057.
42. Shao, Y.; Wang, J.; Engelhard, M.; Wang, C.; Lin, Y. Facile and Controllable Electrochemical Reduction of Graphene Oxide and Its Applications. *J. Mater. Chem.* **2010**, *20*, 743–748.
43. Song, J.; Cheng, L; Liu, A.; Yin, J.; Kuang, M.; Duan, H. W. Plasmonic Vesicles of Amphiphilic Gold Nanocrystals: Self-Assembly and External-Stimuli-Triggered Destruction. *J. Am. Chem. Soc.* **2011**, *133*, 10760–10763.
44. Cheng, L.; Song, J.; Yin, J.; Duan, H. W. Self-Assembled Plasmonic Dimers of Amphiphilic Gold Nanocrystals. *J. Phys. Chem. Lett.* **2011**, *2*, 2258–2262.
45. Jasuja, K.; Berry, V. Implantation and Growth of Dendritic Gold Nanostructures on Graphene Derivatives: Electrical Property Tailoring and Raman Enhancement. *ACS Nano* **2009**, *3*, 2358–2366.
46. Lee, J.; Shim, S.; Kim, B.; Shin, H. S. Surface-Enhanced Raman Scattering of Single- and Few-Layer Graphene by the Deposition of Gold Nanoparticles. *Chem.—Eur. J.* **2011**, *17*, 2381–2387.
47. Bard, A. J.; Faulkner, L. R. *Electrochemical Methods: Fundamentals and Applications [M]*, 2nd ed.; Wiley: New York, 2001.
48. Brennan, J. L.; Branham, M. R.; Hicks, J. F.; Osisek, A. J.; Donkers, R. L.; Georganopoulou, D. G.; Murray, R. W. Electron Hopping Dynamics in Monolayer-Protected Au Cluster Network Polymer Films by Rotated Disk Electrode Voltammetry. *Anal. Chem.* **2004**, *76*, 5611–5619.
49. Mirkhalaf, F.; Schiffrin, D. J. Electrocatalytic Oxygen Reduction on Functionalized Gold Nanoparticles Incorporated in a Hydrophobic Environment. *Langmuir* **2010**, *26*, 14995–15001.
50. Zhao, J.; Bradbury, C. R.; Fermín, D. J. Long-Range Electronic Communication between Metal Nanoparticles and Electrode Surfaces Separated by Polyelectrolyte Multilayer Films. *J. Phys. Chem. C* **2008**, *112*, 6832–6841.
51. Luo, Y.; Liu, H.; Rui, Q.; Tian, Y. Detection of Extracellular H_2O_2 Released from Human Liver Cancer Cells Based on TiO_2 Nanoneedles with Enhanced Electron Transfer of Cytochrom *c*. *Anal. Chem.* **2009**, *81*, 3035–3041.
52. Liu, A. P.; Peng, S.; Soo, J. C.; Kuang, M.; Chen, P.; Duan, H. W. Quantum Dots with Phenylboronic Acid Tags for Specific Labeling of Sialic Acids on Living Cells. *Anal. Chem.* **2011**, *83*, 1124–1130.